

16. G. Thon, A. Cohen, A. J. Klar, *Genetics* **138**, 29 (1994).
 17. S. I. S. Grewal, M. J. Bonaduce, A. J. Klar, *Genetics* **150**, 563 (1998).
 18. J. Nakayama, J. C. Rice, B. D. Strahl, C. D. Allis, S. I. S. Grewal, *Science* **292**, 110 (2001).
 19. K. Noma, C. D. Allis, S. I. S. Grewal, *Science* **293**, 1150 (2001).
 20. S. I. S. Grewal, A. J. Klar, *Genetics* **146**, 1221 (1997).
 21. J. Nakayama, A. J. Klar, S. I. S. Grewal, *Cell* **101**, 307 (2000).
 22. S. I. S. Grewal, A. J. Klar, *Cell* **86**, 95 (1996).
 23. K. Noma, S. I. S. Grewal, unpublished data.
 24. N. Ayoub, I. Goldshmidt, R. Lyakhovetsky, A. Cohen, *Genetics* **156**, 983 (2000).
 25. G. J. Hannon, *Nature* **418**, 244 (2002).
 26. M. Wassenegeger, *Plant Mol. Biol.* **43**, 203 (2000).
 27. M. Matzke, A. J. M. Matzke, J. M. Kooter, *Science* **293**, 1080 (2001).
 28. L. Aravind, H. Watanabe, D. J. Lipman, E. V. Koonin, *Proc. Natl. Acad. Sci. U.S.A.* **97**, 11319 (2000).
 29. G. Hutvagner, P. D. Zamore, *Curr. Opin. Genet. Dev.* **12**, 225 (2002).
 30. T. Volpe, C. Kidner, I. M. Hall, G. Teng, S. I. S. Grewal, R. A. Martienssen, *Science*, **297**, 1833 (2002).
 31. B. J. Reinhart, D. P. Bartel, *Science*, **297**, 1831 (2002).
 32. A. Akhtar, D. Zink, P. B. Becker, *Nature* **407**, 405 (2000).
 33. A. J. Bannister *et al.*, *Nature* **410**, 120 (2001).
 34. V. Jackson, R. Chalkley, *Biochemistry* **24**, 6930 (1985).
 35. E. Heard *et al.*, *Cell* **107**, 727 (2001).
 36. E. U. Selker, *Cell* **97**, 157 (1999).
 37. M. Pal-Bhadra, U. Bhadra, J. A. Birchler, *Mol. Cell* **9**, 315 (2002).
 38. We thank W. Tansey and J. Rice for critical reading of the manuscript; J. Nakayama, R. Martienssen, and G. Hannon for helpful contributions; D. Bartel for sharing unpublished results; and G. Xiao and Y. Tsukamoto for technical assistance. I.M.H. is an Arnold and Mabel Beckman Fellow and thanks S. Nuñez for her support. Funded by grants from Ellison Medical Foundation and the National Institutes of Health (GM59772) to S.I.S.G. and the Israel Science Foundation (N157/00-1) to A.C.

22 July 2001; accepted 14 August 2002

Published online 5 September 2002;

10.1126/science.1076466

Include this information when citing this paper.

REPORTS

Orbital Ordering Transition in $\text{La}_4\text{Ru}_2\text{O}_{10}$

P. Khalifah,^{1,2*} R. Osborn,³ Q. Huang,^{4,5} H. W. Zandbergen,^{2,6} R. Jin,^{7†} Y. Liu,⁷ D. Mandrus,⁸ R. J. Cava^{1,2}

We report experimental evidence for a full orbital ordering transition in the two-dimensional lanthanum ruthenate $\text{La}_4\text{Ru}_2\text{O}_{10}$. The observable consequences of this orbital ordering include the loss of the Ru local moment, a structural distortion which partitions Ru-O bonds into axially oriented short and long sets, a sharp jump in electrical resistivity, and the opening of a spin gap that is visible in neutron scattering experiments. This is a rare example of a discrete orbital ordering transition in a $4d$ transition metal oxide and demonstrates that orbital effects can have an influence on the properties of layered ruthenates, a family of compounds that notably includes the p -wave superconductor Sr_2RuO_4 and the field-tuned quantum critical metamagnet $\text{Sr}_3\text{Ru}_2\text{O}_7$.

The study of the interplay between orbital, spin, and charge degrees of freedom in transition metal oxides is at the forefront of condensed-matter physics (1). Invariably, the canonical examples of orbitally ordered compounds [including YTiO_3 (2), YVO_3 (3),

KCuF_3 (4), and the perovskite manganites (5–8)] contain $3d$ transition metals because they display large magnetic moments and strong coupling of orbital and charge configurations to local coordination polyhedron geometry. Recently, evidence has been mounting for the importance of orbital physics in perovskite-related structures containing the $4d$ transition metal ruthenium (Ru). Inelastic x-ray scattering experiments have found evidence for partial orbital ordering in the compound Ca_2RuO_4 (9), and theoretical models for treating the orbital effects in this system have been developed (10, 11). Unfortunately, it is difficult to assess the effects of orbital ordering on the properties of Ca_2RuO_4 , because the ordering is estimated to be only 50% complete [the d_{xy} orbital occupancy is augmented from 50 to 75% on cooling from 300 K to 90 K] (9), and the shift of orbital population gradually occurs over a tempera-

ture.

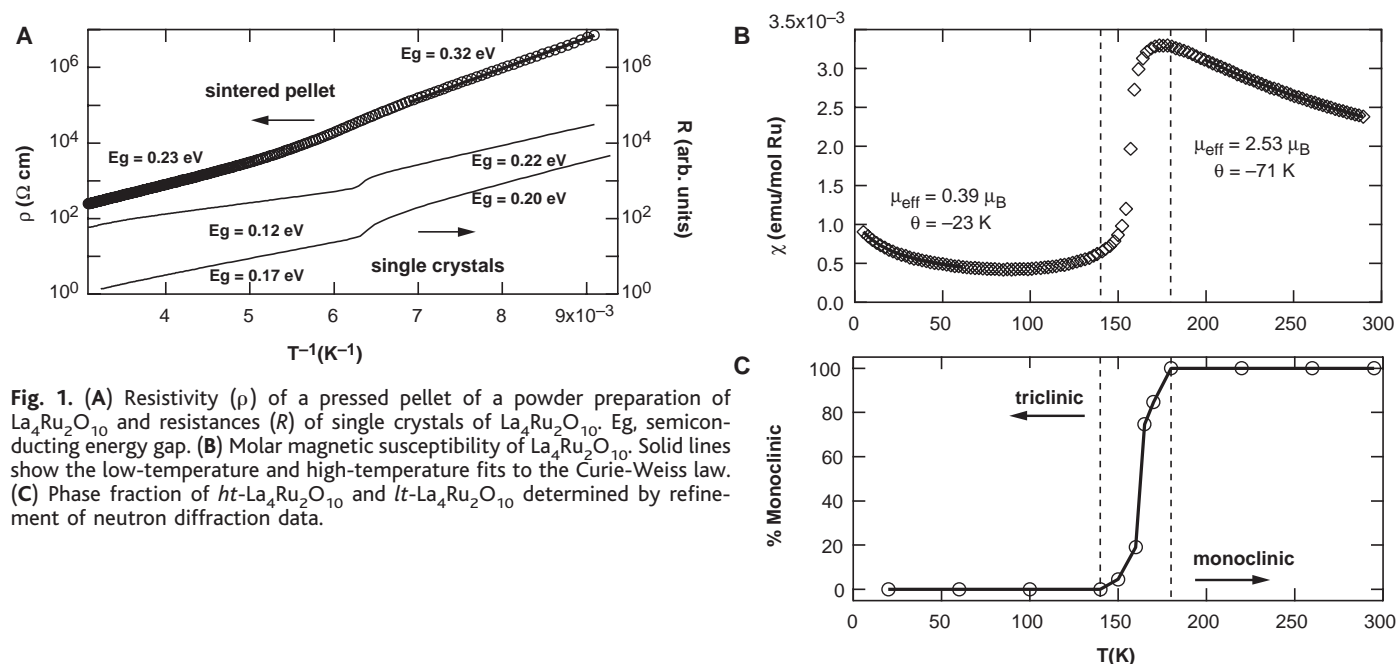


Fig. 1. (A) Resistivity (ρ) of a pressed pellet of a powder preparation of $\text{La}_4\text{Ru}_2\text{O}_{10}$ and resistances (R) of single crystals of $\text{La}_4\text{Ru}_2\text{O}_{10}$. E_g , semiconducting energy gap. (B) Molar magnetic susceptibility of $\text{La}_4\text{Ru}_2\text{O}_{10}$. Solid lines show the low-temperature and high-temperature fits to the Curie-Weiss law. (C) Phase fraction of ht - $\text{La}_4\text{Ru}_2\text{O}_{10}$ and lt - $\text{La}_4\text{Ru}_2\text{O}_{10}$ determined by refinement of neutron diffraction data.

ture range of more than 200 K, judging from the variation of Ru-O bond lengths measured from neutron diffraction refinements (12).

$\text{La}_4\text{Ru}_2\text{O}_{10}$ is a layered ruthenate synthesized in air at 1250°C (13, 14). Despite the black color of $\text{La}_4\text{Ru}_2\text{O}_{10}$ powders and crystals, resistivity measurements show that this compound is nonmetallic. We observed two different semiconducting regimes in $\text{La}_4\text{Ru}_2\text{O}_{10}$ (Fig. 1A), with an increase in the Arrhenius activation energy on cooling below 160 K. The sharp change in the behavior of the resistivity of

$\text{La}_4\text{Ru}_2\text{O}_{10}$ below 160 K indicates a discrete transition between two distinct electronic states.

The stoichiometry of $\text{La}_4\text{Ru}_2\text{O}_{10}$ dictates a Ru^{4+} formal oxidation state and a d^4 configuration. The expected $S = 1$ low spin moment of the Ru atoms is confirmed by fits of high-temperature (high- T) magnetic susceptibility data (Fig. 1B) to a modified Curie-Weiss law [$\chi = \chi_0 + C/(T - \theta)$], which give an effective moment (μ_{eff}) of 2.52 bohr magnetons (μ_B), an antiferromagnetic Curie-Weiss θ of -70 K, and a small temperature-independent χ_0 of 1.8×10^{-4} electromagnetic units (emu) per mole of Ru. Although the high-temperature data conform to expectations, there is a precipitous drop in the magnetic susceptibility of $\text{La}_4\text{Ru}_2\text{O}_{10}$ below 160 K, precisely where the crossover in the semiconducting activation energy was observed. Below this transition, the local moment paramagnetism disappears, and the behavior of $\text{La}_4\text{Ru}_2\text{O}_{10}$ is essentially that of a temperature-independent paramagnet, with a slight upturn at the lowest temperatures due to small amounts of free intrinsic spins or extrinsic impurity spins. The susceptibility can be fit to a modified Curie-Weiss law, albeit with a greatly reduced magnetization ($\mu_{\text{eff}} = 0.38 \mu_B$, $\theta = -23$ K, and $\chi_0 = 2.3 \times$

10^{-4} emu/mol of Ru). In either case, it is clear that the magnetic moment of $\text{La}_4\text{Ru}_2\text{O}_{10}$ is extinguished on cooling below the transition temperature. Field-cooled and zero-field cooled data (15) are indistinguishable. No field dependence of the normalized susceptibility is observed at applied fields of up to 9 T.

The discovery of the magnetic and resistivity transitions in $\text{La}_4\text{Ru}_2\text{O}_{10}$ prompted a search for a concurrent structural transition. When crystals of $\text{La}_4\text{Ru}_2\text{O}_{10}$ are cooled below the magnetic transition temperature, a reversible twinning transition sets in, indicating a change in space group symmetry. The space group symmetry, unit cell, and the approximate atomic positions were extracted from measurements on twinned single crystals. These data were used as the starting point of powder neutron diffraction structural refinements at temperatures above, below, and in the vicinity of the magnetic transition. The symmetry of $\text{La}_4\text{Ru}_2\text{O}_{10}$ was found to be monoclinic (space group $P2_1/c$, no. 14) above 170 K and triclinic ($P\bar{1}$, no. 2) below 150 K, and a mixture of the two phases was present at intermediate temperatures. The magnetic and structural transitions had similar temperature dependencies and were closely correlated (Fig. 1C). Despite the change in space group symmetry, the low-temperature triclinic structure (which will be referred to as *lt*- $\text{La}_4\text{Ru}_2\text{O}_{10}$) and the high-temperature monoclinic structure (*ht*- $\text{La}_4\text{Ru}_2\text{O}_{10}$) remained very similar (Fig. 2A). None of the unit cell dimensions changed by more than 0.5% (<0.04 Å) between 20 and 295 K, and the changes in cell angles and cell volume were also small ($<2.5^\circ$ and $<0.5\%$, respectively). Low-temperature electron diffraction studies showed no evidence of supercell reflections. Although the structural transition in $\text{La}_4\text{Ru}_2\text{O}_{10}$ reflects concurrent changes in the electronic structure of this material, the changes are not due to gross structural changes. Instead, the electronic changes must be driven by specific changes in the nature of the Ru-O interactions.

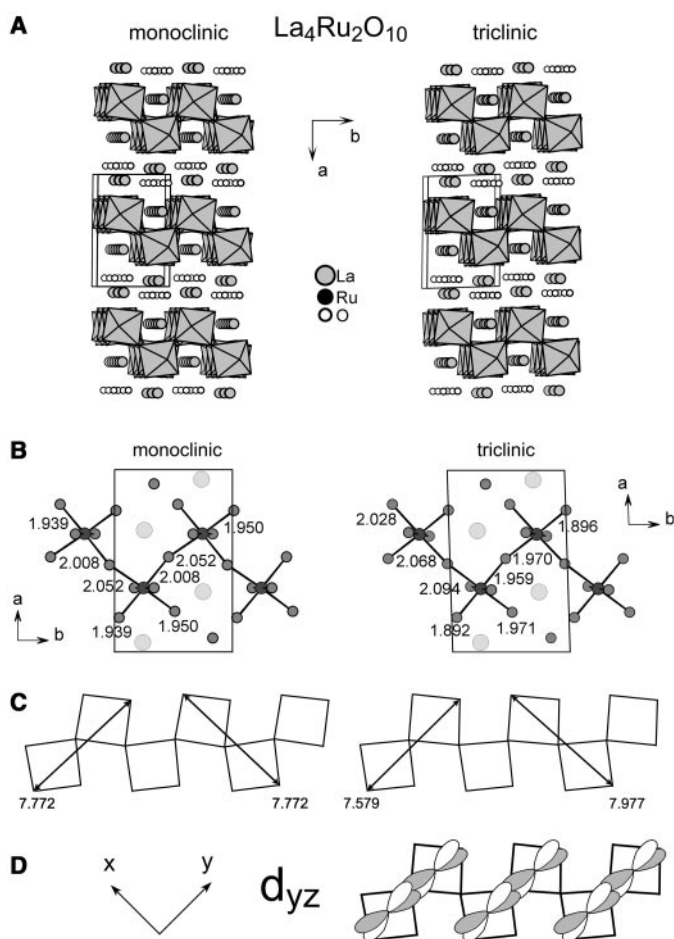
The high- and low-temperature structures of $\text{La}_4\text{Ru}_2\text{O}_{10}$ are closely related to those of the Ruddlesden-Popper-type ruthenates, a family of materials in which orbital effects are believed to play an important role in governing the observed physical properties (9–12, 16). $\text{La}_4\text{Ru}_2\text{O}_{10}$ contains double 110 perovskite planes (Fig. 2A), much as the $n = 2$ Ruddlesden-Popper phase $\text{Sr}_3\text{Ru}_2\text{O}_7$ is built from double 100 perovskite planes. Although both $\text{Sr}_3\text{Ru}_2\text{O}_7$ and $\text{La}_4\text{Ru}_2\text{O}_{10}$ have double-layered structures, there are important differences in their connectivities. Each RuO_6 octahedron in $\text{La}_4\text{Ru}_2\text{O}_{10}$ has corner-sharing connections with four neighboring RuO_6 octahedra, which is one less than the five connections found in $\text{Sr}_3\text{Ru}_2\text{O}_7$. This suggests that $\text{La}_4\text{Ru}_2\text{O}_{10}$ is more electronically similar to the single-layered ($n = 1$) Ruddlesden-Popper phases Sr_2RuO_4 and Ca_2RuO_4 , which also have four nearest-

¹Department of Chemistry, ²Princeton Materials Institute, Princeton University, Princeton, NJ 08540, USA. ³Materials Science Division, Argonne National Laboratory, Argonne, IL 60439, USA. ⁴NIST Center for Neutron Research, National Institute of Standards and Technology, Gaithersburg, MD 20899, USA. ⁵Department of Materials and Nuclear Engineering, University of Maryland, College Park, MD 20742, USA. ⁶National Center for High Resolution Electron Microscopy, Technical University of Delft, Rotterdamsweg 137, 2628AL Delft, The Netherlands. ⁷Department of Physics, The Pennsylvania State University, University Park, PA 16802, USA. ⁸Solid State Division, Oak Ridge National Laboratory, Oak Ridge, TN 37831, USA.

*To whom correspondence should be addressed. E-mail: kpete@ornl.gov

†Present address: Solid State Division, Oak Ridge National Laboratory, Oak Ridge, TN 37831, USA.

Fig. 2. (A) Structure of the monoclinic *ht*- $\text{La}_4\text{Ru}_2\text{O}_{10}$ (left) and triclinic *lt*- $\text{La}_4\text{Ru}_2\text{O}_{10}$ (right) forms of $\text{La}_4\text{Ru}_2\text{O}_{10}$. The black box denotes a single unit cell. Double planes of RuO_6 octahedra (light gray) are the dominant structural feature in both structures. La atoms (medium circles, light) and O atoms (small circles, dark) fill the space between planes in $\text{La}_4\text{Ru}_2\text{O}_{10}$, whereas the Sr atoms in $\text{Sr}_3\text{Ru}_2\text{O}_7$ are not found outside the perovskite planes. (B) Ru-O distances in *ht*- $\text{La}_4\text{Ru}_2\text{O}_{10}$ and *lt*- $\text{La}_4\text{Ru}_2\text{O}_{10}$. (C) Schematic illustrating the distortion occurring in *lt*- $\text{La}_4\text{Ru}_2\text{O}_{10}$ relative to *ht*- $\text{La}_4\text{Ru}_2\text{O}_{10}$. Alternating elongation and compression occur along the diagonals of *lt*- $\text{La}_4\text{Ru}_2\text{O}_{10}$. (D) Ferro-orbital ordering scheme for *lt*- $\text{La}_4\text{Ru}_2\text{O}_{10}$. If the d_{yz} orbitals (shown superimposed on the RuO_6 octahedra) are unoccupied, the y -axis Ru-O bond distances are expected to shrink.



neighbor RuO_6 octahedra. It has been experimentally observed that the partial orbital occupancies of Ca_2RuO_4 vary as a function of temperature (9), a change closely linked to structural distortions (16) and magnetic ordering (10, 11, 17).

On crossing the 160 K transition in $\text{La}_4\text{Ru}_2\text{O}_{10}$, there are large changes in the Ru-O bonding, which indicate a change in orbital populations. When the distance across the entire O-Ru-O-Ru-O chain along the zig-zag diagonals is measured, the *lt*- $\text{La}_4\text{Ru}_2\text{O}_{10}$ structure is found to have alternating distances of and 7.977 and 7.579 Å, in contrast to the uniform distance of 7.772 Å found in *ht*- $\text{La}_4\text{Ru}_2\text{O}_{10}$ (Fig. 2B). A detailed look shows that the four collinear Ru-O bonds in *lt*- $\text{La}_4\text{Ru}_2\text{O}_{10}$ differ by 0.10 Å from the corresponding bond along the opposite diagonal axis (a 5% change) and have each been distorted by an average of 0.05 Å from their monoclinic counterpart (Fig. 2C). The systematic 5% difference in bond lengths is immense in the context of 4d transition metal oxides, which do not typically have the large Jahn-Teller distortions commonly found in 3d transition metal oxides. Furthermore, the axially oriented change in bond lengths is a strong indication of a change in the occupation of the Ru orbitals. The shortest Ru-O bonds are expected to lie along the axes of unoccupied orbitals because of the minimized repulsion between Ru *d* and O *p* orbitals. If the *x* axis of the Ru in *lt*- $\text{La}_4\text{Ru}_2\text{O}_{10}$ is taken to be along the long Ru-O bonds and the *y*-axis is taken to be along the short Ru-O bonds, then the distortion of the RuO_6 octahedra reflects an increased occupancy of the d_{xz} orbitals and a decreased occupancy of the d_{yz} orbitals. The greatest possible compression of Ru-O bond lengths along the *y* axis will occur when the d_{yz} orbitals are unoccupied (Fig. 2D), giving an effective Ru configuration of $d_{xy}^2 d_{xz}^2$. The structural distortion in $\text{La}_4\text{Ru}_2\text{O}_{10}$ is therefore the physical manifestation of an orbital ordering transition in which the d_{yz} orbital is selectively depopulated.

The $\text{La}_4\text{Ru}_2\text{O}_{10}$ orbital ordering transition naturally explains the unusual magnetic transition, as illustrated in Fig. 3. $\text{La}_4\text{Ru}_2\text{O}_{10}$ contains Ru^{4+} ions at all temperatures, which leaves four *d* electrons to fill the t_{2g} -derived bands. At temperatures above the structural and magnetic transition, *ht*- $\text{La}_4\text{Ru}_2\text{O}_{10}$ is a paramagnetic insulator, with the two unpaired t_{2g} electrons in its triply degenerate t_{2g} orbitals. Hund's rules predict an electron configuration of $d_{xy}^2 d_{xz}^1 d_{yz}^1$, $d_{xy}^1 d_{xz}^2 d_{yz}^1$, or $d_{xy}^1 d_{xz}^1 d_{yz}^2$. The two unpaired electrons in these degenerate states result in the 2.53 μ_B moment ($S = 1$) observed in the Curie-Weiss fit of the magnetic susceptibility. Upon cooling through the transition temperature, the orbital ordering transition induces systematic bond distortions that drive the monoclinic \rightarrow triclinic structural phase transition. The "ferro-orbital" nature of the transition results in the systematic compression of Ru-O

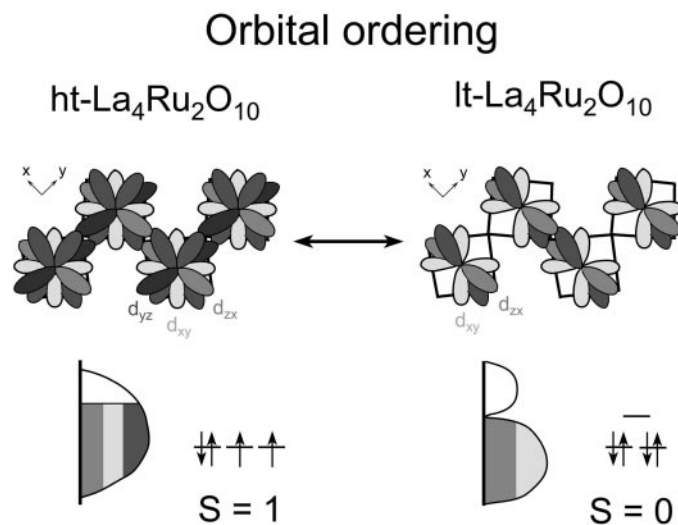


Fig. 3. Schematic showing the effects of a completely empty d_{yz} orbital on the t_{2g} -derived energy bands and on the magnetism of *lt*- $\text{La}_4\text{Ru}_2\text{O}_{10}$.

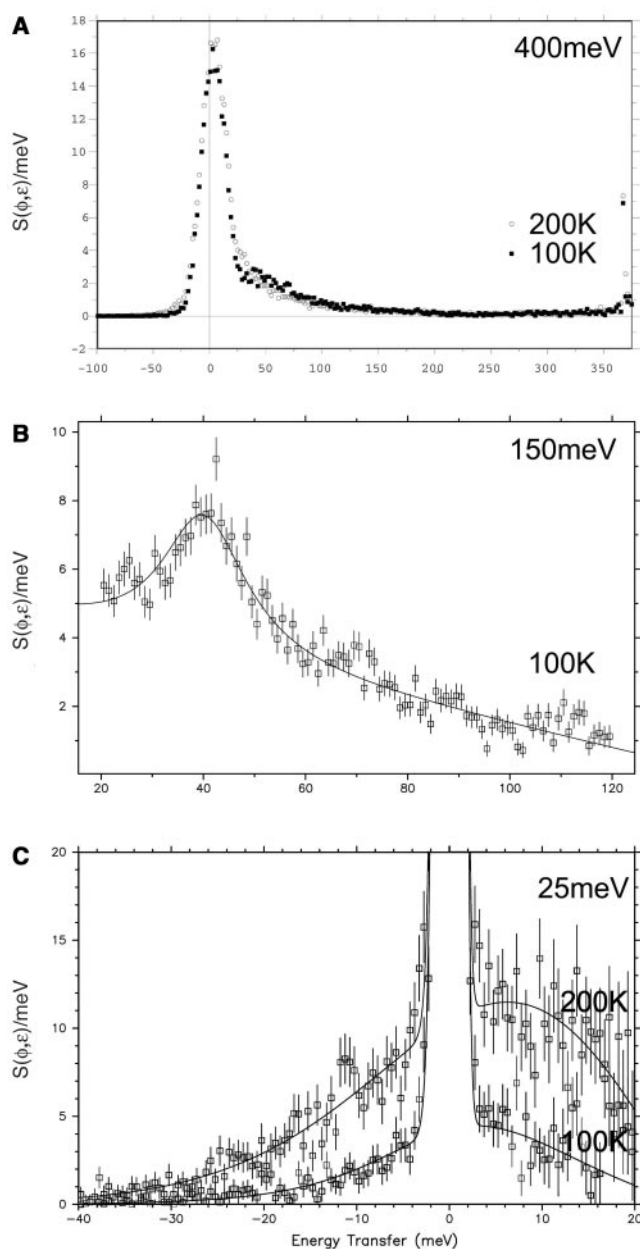


Fig. 4. Inelastic neutron scattering results for *ht*- $\text{La}_4\text{Ru}_2\text{O}_{10}$ (200 K) and *lt*- $\text{La}_4\text{Ru}_2\text{O}_{10}$ (100 K) at incident energies of (A) 400, (B) 150, and (C) 25 meV. $S(\phi/\varepsilon)$ is the neutron scattering law measured at an average scattering angle $\phi = 5^\circ$, as a function of energy transfer (ε) in units of mbarns/sr/meV per formula unit (i.e., two Ru atoms). The solid lines are fits to inelastic (B) and quasi-elastic (C) Lorentzian line shapes using parameters given in the text, with corrections for self-shielding and the Ru^{4+} form factor.

bonds along the y axis (110), raising the energy of d_{yz} orbitals well above the level of the d_{xz} and d_{xy} orbitals. Instead of a two-thirds-filled set of threefold-degenerate t_{2g} orbitals, ht -La₄Ru₂O₁₀ contains one nearly full doubly degenerate band and one nearly empty nondegenerate band (electron configuration $d_{xy}^2 d_{xz}^2 d_{yz}^0$). This results in virtually all of the d electrons in ht -La₄Ru₂O₁₀ being paired and in the loss of the $S = 1$ magnetic moment.

The conclusion that the magnetic transition in La₄Ru₂O₁₀ is driven by orbital ordering is supported by other measurements. Powder neutron diffraction data rule out antiferromagnetic ordering as the cause of the magnetic transition, because of the absence of supercell reflections in the low-temperature data and because of the successful fitting of the observed data without including magnetic scattering. In some systems such as NdNiO₃ (18), sharp magnetic transitions are induced by metal-insulator transitions. However, this is certainly not the case in La₄Ru₂O₁₀, which is semiconducting both above and below the magnetic transition.

The formation of a spin gap in the orbitally ordered state is confirmed by inelastic neutron scattering experiments on powder samples (Fig. 4). These neutron scattering experiments are able to directly probe the nature of magnetic excitations and can readily resolve the fundamental magnetic changes upon cooling through the 160 K transition. Data on ht -La₄Ru₂O₁₀ were collected at 200 K, whereas data on lt -La₄Ru₂O₁₀ were collected at 100 K. Initial experiments using 400-meV neutrons allow the broad features of La₄Ru₂O₁₀ to be probed. Even on this large energy scale, it can be seen that there are substantial differences between lt -La₄Ru₂O₁₀ and ht -La₄Ru₂O₁₀. The response of ht -La₄Ru₂O₁₀ is featureless except for the broad quasi-elastic peak centered at zero energy transfer (Fig. 4A). This is not the case for lt -La₄Ru₂O₁₀, which exhibits a second peak around 40 meV, which can be more clearly resolved when probed with 150-meV neutrons (Fig. 4B). In addition, the quasi-elastic scattering of lt -La₄Ru₂O₁₀ is greatly reduced, as can be seen in data collected at 25 meV (Fig. 4C).

The magnetic contribution to the scattering in ht -La₄Ru₂O₁₀ is best fit to a purely quasi-elastic peak with a width of 40.5 ± 5.4 meV. On the other hand, the fit to the scattering from lt -La₄Ru₂O₁₀ shows a significantly reduced quasi-elastic peak (with a width of 16.2 ± 2.6 meV) and a new inelastic peak centered at 41.2 ± 0.6 meV and with a width of 8.6 ± 1.6 meV. The purely quasi-elastic response of ht -La₄Ru₂O₁₀ is characteristic of gapless systems with a strongly fluctuating local moment. In contrast, the 40-meV inelastic peak is a strong indicator that a gap is present in lt -La₄Ru₂O₁₀. The reduced quasi-elastic scattering of lt -La₄Ru₂O₁₀ relative to ht -La₄Ru₂O₁₀, which results from the opening of a discrete spin gap, is seen in the 25-meV scan (Fig. 4C). It is expect-

ed that the magnetic quasi-elastic scattering in lt -La₄Ru₂O₁₀ would be further or even completely reduced at temperatures well below 100 K, where thermal excitations across the 40-meV gap are no longer contributing to the quasi-elastic peak.

The structural evidence for an orbital ordering transition in La₄Ru₂O₁₀ is strongly supported by magnetic susceptibility and inelastic neutron-scattering measurements. Although previous studies hinted at the importance of orbital effects, La₄Ru₂O₁₀ provides the first realization of a full orbital ordering transition among ruthenates. There is a strong possibility that many of the phenomena seen in orbitally ordered manganites (such as charge ordering, stripe formation, and colossal magnetoresistance) may now also be found in doped layered ruthenates. Given the large differences in magnetism between $3d$ and $4d$ transition metals, there will be important new opportunities to gain insights into the phenomena associated with orbital ordering through their comparison.

References and Notes

1. Y. Tokura, N. Nagaosa, *Science* **288**, 462 (2000).
2. H. Ichikawa, J. Akimitsu, M. Nishi, K. Kakurai, *Physica B* **281-2**, 482 (2000).
3. G. R. Blake, T. T. M. Palstra, Y. Ren, A. A. Nugroho, A. A. Menovsky, *Phys. Rev. Lett.* **87**, 245501 (2001).

4. A. E. Nikiforov, S. Y. Shashkin, M. L. Levitan, T. H. Agamalyan, *Phys. Status Solidi B* **118**, 419 (1983).
5. T. Mizokawa, D. I. Khomskii, G. A. Sawatzky, *Phys. Rev. B* **60**, 7309 (1999).
6. A. M. Goldman, *Science* **274**, 1630 (1996).
7. A. Moreo, S. Yunoki, E. Dagotto, *Science* **283**, 2034 (1999).
8. Y. D. Chuang, A. Gromko, D. Dessau, T. Kimura, Y. Tokura, *Science* **292**, 1509 (2001).
9. T. Mizokawa *et al.*, *Phys. Rev. Lett.* **87**, 077202 (2001).
10. T. Hotta, E. Dagotto, *Phys. Rev. Lett.* **88**, 017201 (2002).
11. V. I. Anisimov, I. A. Nekrasov, D. E. Kondakov, T. M. Rice, M. Sigrist, *Eur. Phys. J. B* **25**, 191 (2000).
12. O. Friedt *et al.*, *Phys. Rev. B* **58**, 847 (1998).
13. P. Khalifah, Q. Huang, H. Zandbergen, D. M. Ho, R. J. Cava, in preparation.
14. Materials and methods are available as supporting material on Science Online.
15. P. Khalifah *et al.*, data not shown.
16. M. Braden, G. Andre, S. Nakatsuji, Y. Maeno, *Phys. Rev. B* **58**, 847 (1998).
17. Z. Fang, K. Terakura, *Phys. Rev. B* **64**, 020509 (2001).
18. M. Imada, A. Fujimori, Y. Tokura, *Rev. Mod. Phys.* **70**, 1039 (1998).
19. Supported by NSF grants DMR-9725979 and 9974327 and by the U.S. Department of Energy, Office of Science, under contract W-31-109-ENG-38. P.K. gratefully acknowledges support from an NSF graduate fellowship. The authors thank L. Mattheiss for helpful discussions.

Supporting Online Material

www.sciencemag.org/cgi/content/full/297/5590/2237/DC1
Materials and Methods

28 June 2002; accepted 20 August 2002

Collapse of a Degenerate Fermi Gas

Giovanni Modugno,* Giacomo Roati, Francesco Riboli, Francesca Ferlaino, Robert J. Brecha, Massimo Inguscio

A degenerate gas of identical fermions is brought to collapse by the interaction with a Bose-Einstein condensate. We used an atomic mixture of fermionic potassium-40 and bosonic rubidium-87, in which the strong interspecies attraction leads to an instability above a critical number of particles. The observed phenomenon suggests a direction for manipulating fermion-fermion interactions on the route to superfluidity.

Experimental research on ultracold atoms has highlighted the marked differences of bosonic and fermionic dilute quantum gases in the basic properties (I). In the case of a degenerate Fermi gas, confined in a harmonic external potential, the Pauli exclusion principle forbids the multiple occupation of a single quantum state and leads to a strong effective repulsion between the identical atoms. The fermions are arranged in the trap in a cloud with relatively large spatial distribution and

large kinetic energy, which can be interpreted as being the result of an outward “Fermi pressure” (2, 3). This is a general property of any degenerate Fermi system; for instance, it is the mechanism that stabilizes white dwarfs and neutron stars against gravitational collapse. As a result of this pressure, a dilute atomic Fermi gas is only weakly affected by the actual interactions between particles. Conversely, a Bose-Einstein condensate (BEC) occupies only the ground state of the trap, with a narrow spatial distribution, and the presence of interactions can strongly alter its structure. Indeed, a repulsive interaction broadens the density distribution, whereas an attractive interaction can lead to a collapse for a sufficiently large number of atoms, as observed for lithium (4) and rubidium (5).

European Laboratory for Nonlinear Spectroscopy, Università di Firenze, and Istituto Nazionale per la Fisica della Materia (INFM), Via Nello Carrara 1, 50019 Sesto Fiorentino, Italy.

*To whom correspondence should be addressed. E-mail: modugno@lens.unifi.it